Phase Measurement in Electron Microscopy Using the Transport of Intensity Equation

Kazuo Ishizuka, and Brendan Allman*
*HREM Research Inc, *IATIA Ltd*
ishizuka@hremresearch.com

Introduction

Although many samples in electron microscopy are phase objects, as in the case of optical microscopy, we cannot directly measure phase modulation by microscopy. Dennis Gabor proposed a technique called in-line holography to record both amplitude and phase information at the rather early stage of electron microscopy (in 1947). With the development of highly coherent field emission electron sources, another type of holography, off-axis holography, became available for electrons. However, holography cannot be applied to general cases, since there is a requirement for a vacuum region where the reference wave passes through. Realizing a Zernike-type phase plate, as used in optical microscopy, has also been difficult in electron microscopy. Therefore, imaging conditions proposed by Scherzer have been utilized in electron microscopy, where an approximate phase plate is realized by introducing a defocus in the presence of spherical aberration.

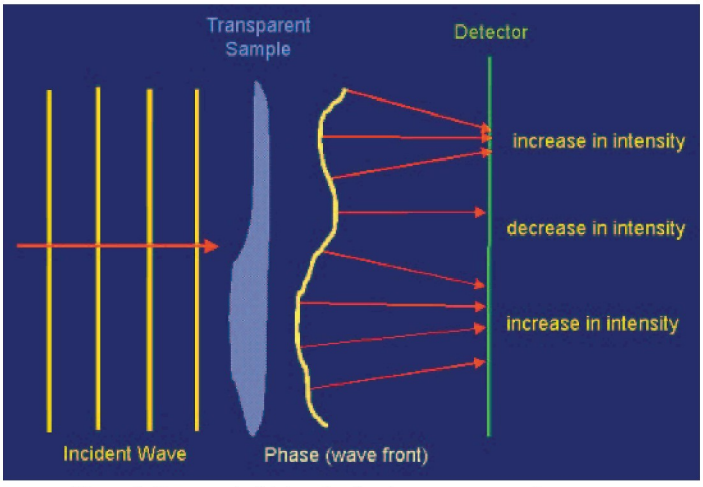

Figure 1. Transport of intensity due to wave propagation.

About twenty years ago, Teague [1] derived an equation for wave propagation in terms of phase and intensity distributions, and showed that the phase distribution may be determined by measuring only the intensity distributions. We call this equation the Transport of Intensity Equation (TIE). The TIE was recently applied successfully to transmission electron microscopy at medium resolution to observe static potential distributions of biological and non-biological samples or to measure magnetic fields. It has been very recently verified that the TIE will be applicable to even atomic resolution images. In this report we introduce the basic concept of the TIE and show some results obtained from material science specimens.

What is the Transport of Intensity Equation?

The propagation of a wave is schematically illustrated in Fig. 1. Here, a plane wave impinges a specimen, which distorts both the amplitude and the phase of the incoming wave. For a phase object, the amplitude change is negligible, and the information concerning the specimen is encoded in the phase modulation (wave front deformation) only. Thus, the amplitude of the exit wave is almost constant immediately below the specimen exit surface. However, when a wave propagates through empty space, the amplitude at some places will increase and at other places the amplitude will decrease, according to the phase modulation induced by the specimen. The transport of intensity equation says that we will be able to determine phase information from intensity measurements only.

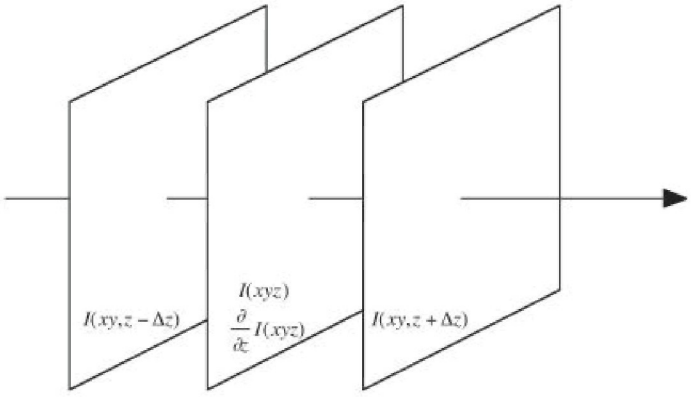

Figure 2. An experimental situation, where we have to estimate the intensity derivative at the center plane.

Mathematically, the TIE for electrons exactly corresponds to the Schrödinger equation for high-energy electrons in free space. Namely, the following TIE

$$\frac{2\pi}{\lambda}\frac{\partial}{\partial z}I(xyz) = -\nabla_{xy}\bullet\left(I(xyz)\nabla_{xy}\phi(xyz)\right) \qquad (1)$$

is obtained, when we replace the complex wave function ψ in the Schrödinger equation with the two real functions, I and φ, which represent the intensity and phase distributions respectively. Here, $\partial I/\partial z$ is an intensity derivative along the wave propagation direction, and ∇^2_{xy} is a two-dimensional Laplacian.

Thus, we have to estimate an intensity derivative with respect to z as accurately as possible. An accurate estimate of the intensity derivative may be obtained by a difference of image intensities measured at a sufficiently close interval. However, this does not work in practice, since non-negligible noise always exists in the images. Therefore, a large defocus step is preferable to increase the signal over the noise in the intensity difference. For the symmetric three-image case as shown in Fig. 2, where the three images are recorded with the same defocus distance, the intensity derivative may be given by an intensity difference between the two side planes as follows.

$$\frac{I(z+\varepsilon)-I(z-\varepsilon)}{2\varepsilon} = \frac{\partial I}{\partial z} + O(\varepsilon^2) \qquad (2)$$

We may note that all of the even order terms of two Taylor expansions for $I(z+\varepsilon)$ and $I(z-\varepsilon)$ are cancelled out, and thus the simple difference will give a good estimate of the derivative. Nevertheless, the images taken with a too large defocus step

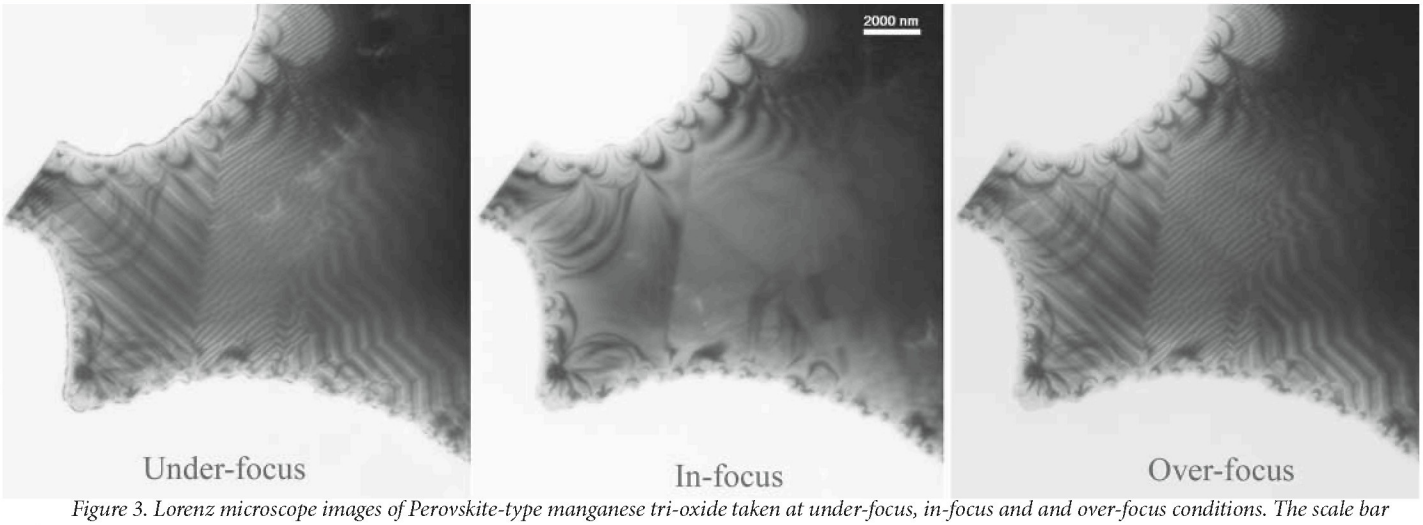

Figure 3. Lorenz microscope images of Perovskite-type manganese tri-oxide taken at under-focus, in-focus and and over-focus conditions. The scale bar is 2 micron.

will give a poor estimate of the derivative.

An upper limit of the defocus distance that gives a good estimate of the derivative in the case of the symmetric three images may be given by

$$\frac{\left(\pi \lambda \varepsilon g_{\max}^2\right)^2}{3!} \leq c \ll 1 \qquad (3)$$

where g_{max} is the highest spatial frequency included in the image, and c is a small number, say 0.25. Table 1 will give an idea of the defocus limits for some resolutions and accelerating voltages. The upper defocus limit is proportional to the square of the resolution, and inversely proportional to the wavelength. We may note that the upper defocus limit for a resolution of 0.14 nm assuming 400 kV electrons is 9.5 nm. Since such a large defocus step will give a sufficient intensity change even for high-resolution images, the TIE will be applicable to atomic resolution images as shown in the second example below.

Table 1. Typical upper limits of defocus for the three-image case

d_{min}	$\pi\lambda(2\varepsilon)$	100 kV	200 kV	400 kV
0.14 nm	4.90 x10^{-2}	4.2 nm	6.2 nm	9.5 nm
0.2	9.80 x 10^{-2}	8.4	12.4	19.0
1	2.45	211	311	474
10	2.45 x10^{2}	21.1 μm	31.1 μm	47.4 μm
100	2.45 x10^{4}	2.11 mm	3.11 mm	4.74 mm

This table shows typical upper limits of defocus distance (2ε) between under-focus and over-focus images for some resolutions d_{min} and accelerating voltages. Here, we assume an upper error limit as c=0.25.

Examples

To demonstrate the applicability of the TIE to measuring the phase information of an exit wave function, we will show two results from material sciences.

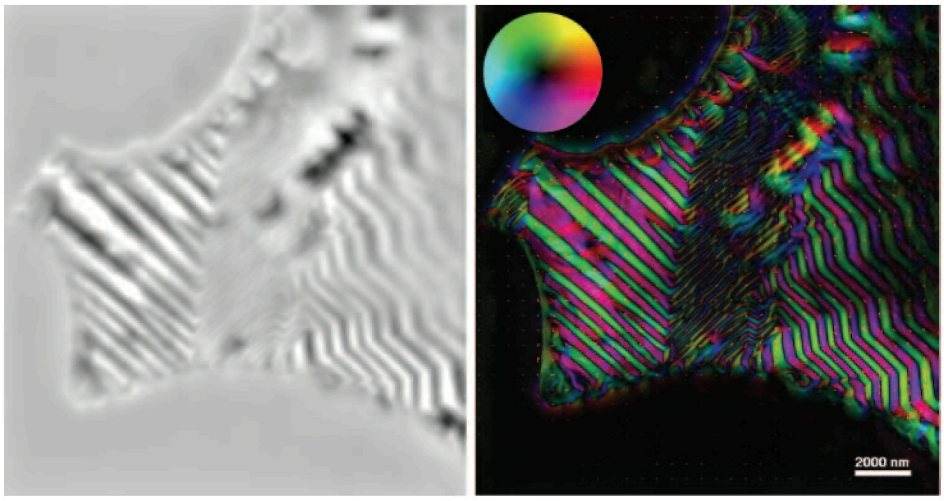

Figure 4. (left) Phase distribution and (right) magnetization vector map.

Observation of magnetization patterns

Figure 3 shows in-focus, under-focus and over-focus images taken from a Perovskite-type manganese tri-oxide ($Pr_{1-x}(Ca_{1-y}, Sr_y)_xMnO_3$ (x=0.45, y=0.4)) using a Lorenz microscope (Hitachi HF-3000L) at about 2k magnification. This material undergoes a transformation from a paramagnetic (high-temperature) phase to a ferromagnetic (low-temperature) phase at around 220°K. The defocus distance from the in-focus plane is about 2 mm. We note that the images taken at under-focus and over-focus conditions show bright and dark contrast bands at domain boundaries, indicative of a phase contrast effect. Figure 4 shows the restored phase and a magnetization vector map obtained by a gradient of the phase distribution. When we compare it with the color wheel, it is clear that magnetization directions are parallel to the elongated domain direction. It is also clear that the wide (180 degree) domains and the narrow (stripe) domains magnetize perpendicular to each other.

Observation of atomic structure with spherical aberration correction

Figure 5 shows small parts of three images selected from a focal series of twenty high-resolution images of Si3N4 taken at a rather large under-focus from 280 nm to 240 nm to prevent

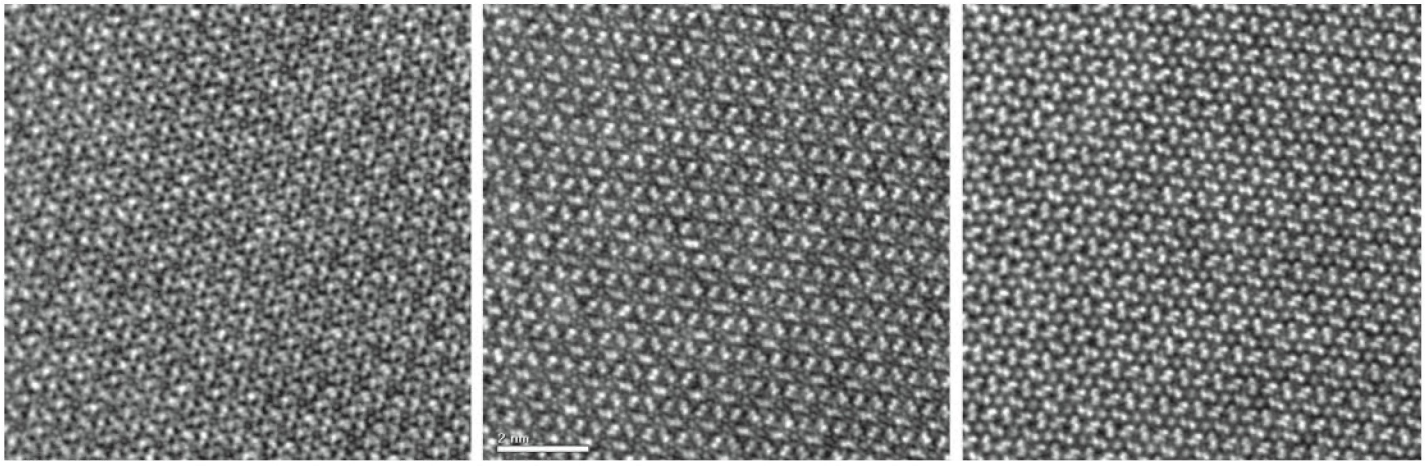

Figure 5. Small parts of under-focus, in-focus (center) and over-focus images of Si_3N_4. The scale bar is 2 nm.

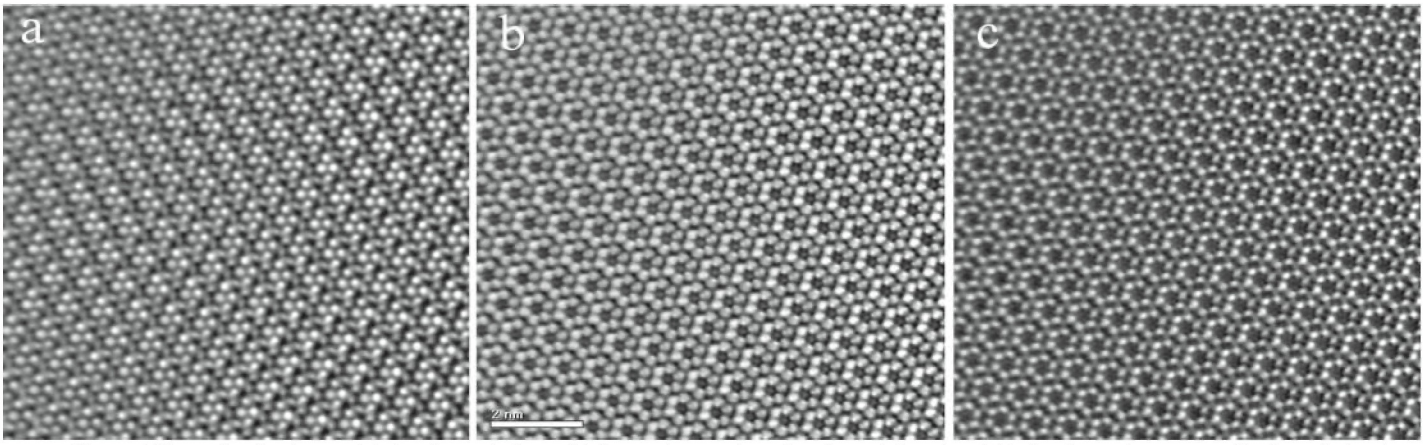

Figure 6. Phase distributions at (a) the observed plane, (b) the specimen exit surface (zero-defocus) and (c) the plane where an amplitude variation is minimal. The scale bar is 2 nm.

attenuation at high spatial frequency due to spatial coherency. These images were obtained at NCEM, Berkeley using a Philips CM300 equipped with a field emission gun. The defocus distance between the under and over-focus images is almost 11.6 nm. Figure 6(a) shows a reconstructed phase at the plane of the center image, namely around 270 nm under-focus from the sample. Using this phase distribution and the observed image intensity, we can now reconstruct a complex wave front at this image plane.

Figure 6(b) shows the phase distribution at the specimen exit surface (zero-defocus) obtained by back-propagating the wave front to the specimen plane. Here, Fourier filtering was employed to remove small heterogeneous contrast. It may be noted that we can correct spherical aberration as well as transfer attenuation due to temporal and spatial partial coherency during the back-propagation. Figure 6(c) shows the phase distribution at the plane where the amplitude variation is minimal. The phase maps shown in Fig. 6 (b) and (c) bear a striking resemblance to the results reported by Ziegler *et al.* [2], where the whole set of twenty images is used to retrieve the wave field with the MAL technique.

The image processing presented here was performed by using QPt for DigitalMicrograph [3].

Conclusions

In this report we have clarified the theoretical aspects of the TIE and shown some materials science examples. The TIE for electrons exactly corresponds to the Schrödinger equation for high-energy electrons in free space, and thus the TIE can be applied not only to a weak phase object, but also to strongly scattering objects. It may be surprising that we can reconstruct an exit wave function at atomic resolution, and then correct spherical aberration using only three images.

Acknowledgements

The authors greatly acknowledge Christian Kisielowsky and Masaya Uchida for kindly providing us high-resolution images of Si_3N_4 and Lorenz images of manganese tri-oxide, respectively.

References

[1] M.R. Teague, J. Opt. Soc. Am. 73 (1983) 1434-1441: Deterministic phase retrieval: a Green's function solution.

[2] A. Ziegler, C. Kisielowski, R.O. Ritchie, Acta Materialia 50 (2002) 567-574: Imaging of the crystal structure of silicon nitride at 0.8 Angstrom resolution.

[3] HREM Research Inc, Higashimatsuyama, 355-0055 Japan; www.hremresearch.com.